JACS
JOURNAL OF THE AMERICAN CHEMICAL SOCIETY
Communication
pubs.acs.org/JACS

Proton Conduction in a Phosphonate-Based Metal–Organic Framework Mediated by Intrinsic "Free Diffusion inside a Sphere"

Simona Pili,[†] Stephen P. Argent,[‡] Christopher G. Morris,[‡,§] Peter Rought,[†] Victoria García-Sakai,[⊥] Ian P. Silverwood,[⊥] Timothy L. Easun,[∥] Ming Li,[#] Mark R. Warren,[§] Claire A. Murray,[§] Chiu C. Tang,[§] Sihai Yang,*[,†] and Martin Schröder*[,†]

[†]School of Chemistry, University of Manchester, Oxford Road, Manchester M13 9PL, U.K.
[‡]School of Chemistry, University of Nottingham, University Park, Nottingham NG7 2RD, U.K.
[§]Diamond Light Source, Harwell Science and Innovation Campus, Oxfordshire OX11 0DE, U.K.
[⊥]ISIS Pulsed Neutron and Muon Source, STFC Rutherford Appleton Laboratory, Chilton, Oxfordshire OX11 0QX, U.K.
[∥]School of Chemistry, Cardiff University, Cardiff CF10 3XQ, U.K.
[#]Department of Mechanical, Materials and Manufacturing Engineering, University of Nottingham, University Park, Nottingham NG7 2RD, U.K.

Supporting Information

ABSTRACT: Understanding the molecular mechanism of proton conduction is crucial for the design of new materials with improved conductivity. Quasi-elastic neutron scattering (QENS) has been used to probe the mechanism of proton diffusion within a new phosphonate-based metal–organic framework (MOF) material, MFM-500(Ni). QENS suggests that the proton conductivity (4.5×10^{-4} S/cm at 98% relative humidity and 25 °C) of MFM-500(Ni) is mediated by intrinsic "free diffusion inside a sphere", representing the first example of such a mechanism observed in MOFs.

Fuel cells represent an appealing option as alternative clean energy systems,[1] and technologies based upon polymer electrolyte membrane fuel cells (PEMFCs) are used widely in portable applications. The design and synthesis of new proton-conducting materials are of fundamental importance for the development of PEMFCs;[2] currently, commercially used proton conductors are based upon acidic polymers such as Nafion which exhibit high conductivity of 10^{-2} S/cm in the presence of water.[3] However, the amorphous nature of such polymers precludes investigation of the mechanisms and/or pathways for their proton conduction, and thus analysis and feedback in order to improve future materials development are difficult to obtain.[4] Constructed from metal ions and organic linkers, metal–organic framework (MOF) materials often display high surface areas, high porosity, and, more importantly, extended crystalline structures, and significant focus has been placed on their applications in gas storage, separation, and catalysis.[5−7] More recently, MOFs have appeared as promising new candidates as porous materials for proton conduction.[8,9]

Functionalization of the organic linker in MOF materials allows the periodic introduction of acidic groups (e.g., SO_3H, PO_3H_2),[10−12] and their intrinsic porosity enables the loading of additional protonic molecules (e.g., imidazole, histamine) within the pore,[13−15] to yield decorated materials with improved proton conductivity. Most importantly, the crystalline nature of MOFs provides an excellent platform to interrogate possible proton hopping and conduction pathways, thus enabling the construction of structure–activity relationships, which cannot be achieved in polymer-based systems due to their intrinsic lack of long-range order.[1] X-ray crystallographic studies afford average positions of protons within the extended lattice, mostly on O-atoms from hydroxy groups or water molecules. These are often refined by a "riding model" and subject to large uncertainties inherent in these X-ray experiments. Understanding the dynamics of these active protons is of fundamental importance for the design of improved materials. However, gaining such information within porous lattices of MOFs is very challenging, and knowledge on the dynamics of proton diffusion in MOFs is rarely reported.[16] Pulsed field gradient (PFG) NMR is capable of measuring the dynamics of specific species in materials containing intrinsic structural defects. However, PFG-NMR is likely to underestimate the diffusion rate, as it operates on longer time and spatial scales.[17] Here we describe the synthesis and crystal structures of two novel isostructural phosphonate-based MOFs, $[M_3(H_3L)_2(H_2O)_9(C_2H_6SO)_3]$ (M = Ni, Co; H_6L = benzene-1,3,5-*p*-phenylphosphonic acid), denoted as MFM-500(Ni) and MFM-500(Co), respectively (MFM = Manchester Framework Material). MFM-500(Ni) and MFM-500(Co) adopt 2D networks, in which the ligand is only 50% deprotonated ($H_6L \rightarrow H_3L^{3-}$) and bound to the metal ions. This affords free acidic protons from the partially protonated ligand within the lattices of these coordination complexes. The materials show proton conductivities of 4.5×10^{-4} [MFM-500(Ni)] and 4.4×10^{-5} S/cm [MFM-500(Co)] at 98% relative humidity (RH) and 25 °C. Single-crystal X-ray structural analyses reveal a potential proton hopping pathway constructed from the free phosphonic acid groups and coordinated water molecules on the metal centers, subject to uncertainties as discussed above.

Received: February 28, 2016

DOI: 10.1021/jacs.6b02194
J. Am. Chem. Soc. XXXX, XXX, XXX−XXX

More importantly, quasi-elastic neutron scattering (QENS) has been used to investigate the intrinsic mechanism of proton diffusion within MFM-500(Ni), and this study suggests that the proton conduction in MFM-500(Ni) is mediated by the model of "free diffusion inside a sphere" rather than "jump diffusion between sites".

Benzene-1,3,5-*p*-phenylphosphonic acid, H_6L, was synthesized following a literature procedure to afford a white powder in 67% yield.[18] Upon mixing $M(NO_3)_2$ (M = Ni, Co) with H_6L in a 2:1 molar ratio in a solution of H_2O/DMSO/DMF, hexagonal column-shaped single crystals of MFM-500(Ni) and MFM-500(Co) grew within 2 days at 40 °C. Synchrotron single-crystal X-ray diffraction (XRD) reveals that the two materials are isostructural, and both crystallize in the hexagonal space group $P6_3/m$ (Table S1) with a 2D layered structure. The tris-phosphonate ligand, H_3L^{3-}, acts as one type of three-connected node in overlapping pairs of 2D hexagonal (6,3) networks lying in the *ab* plane, in which the other type of three-connected node is a disordered mixture of $[M_1(H_2O)_3(RPO_3H)_3]$ or $[M_2(H_2O)_6(\mu^2\text{-}RPO_3H)_3]$ moieties (Figure 1a). Running down the *c*-axis are stacks of pairs of overlapping

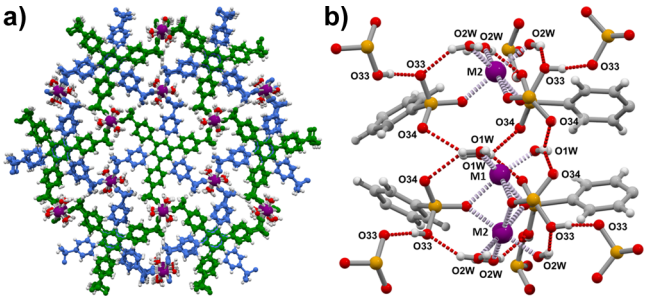

Figure 1. (a) Views of the crystal structure of MFM-500(M) (M = Co, Ni) along the *c*-axis. Minor disorder component sites and DMSO solvent molecules have been omitted for clarity. Overlapping stacks of ligands are blue and green. (b) View of the coordination environment of M_1 and M_2 and the surrounding H-bond network from the single-crystal X-ray structure of MFM-500(Co). C, gray; O, red; P, orange; metal centers, purple; H, white. Coordinate bonds are shown as dashed lilac lines, and H-bonds are shown as dashed red lines.

ligands in which each pair is rotated by 60° with respect to the pairs above and below (ligand separations along the *c*-axis are 3.85 Å between overlapping pairs). Columns of disordered metal centers running along the *c*-axis all have pseudo-octahedral coordination geometries made up of O donors from deprotonated phosphonate hydroxyl groups, neutral water molecules, and partially resolved DMSO molecules. These O donors act as either monodentate or μ^2-bridging ligands, depending on the occupancy of the disordered adjacent metal cation sites. The columns of M_1 and M_2 nodes along the *c*-axis reside in the hexagonal holes within the pairs of offset hexagonal networks above and below them (Figure S1).

In MFM-500(Co), residual electron density peaks were observed for H-atoms on the water molecules and one of the phosphonate hydroxy groups; this has allowed their positions to be refined using suitable geometric restraints, revealing an extensive H-bonding network within and between the columns of metal cations (Figure 1b; Table 1). The H-bond donor–acceptor (D–A) distances range from 2.45 to 3.01 Å and form crossover chains that run between adjacent columns of metal cations via reciprocally disordered H-bonds between symmetry-related phosphonate–hydroxy oxygen atoms O33 (D–A = 2.45 Å). O33 is also involved in disordered H-bonding with a bridging water molecule O2W (D–A = 2.73 Å), while the bridging water molecule O1W donates a bifurcated H-bond to two symmetrically equivalent unbound deprotonated phosphonate–hydroxy oxygen atoms O34 (D–A = 3.01 Å). The passage of H-bond chains along the *c*-axis is interrupted by the presence of a partially occupied disordered DMSO solvent molecule; it is likely that the chains continue through this region conveyed by an unmodeled disorder solvent component. Refinement of the crystal structure of MFM-500(Ni), however, yields no clear electron density peaks on the O donors, thus precluding the inclusion of refined H positions on these atoms. The array of potential H-bond donors and acceptors in MFM-500(Ni) is the same as that in MFM-500(Co), the separation between water oxygen O1W and phosphonate oxygen O34 being slightly shorter [D–A = 3.3013(7) Å in MFM-500(Co) and 2.972(7) Å in MFM-500(Ni)]. The other D–A distances are similar (Table 1).

Thermal gravimetric analysis (TGA) of MFM-500(Ni) and MFM-500(Co) shows similar weight loss steps, with a slightly lower stability observed for MFM-500(Co) (Figure S3). *In situ* variable-temperature PXRD data confirmed a reversible phase transition occurring between 75 and 100 °C for both materials (Tables S3 and S4). This result is consistent with the first step in the TGA plots and is associated with a color change from green to brown for MFM-500(Ni) and from pink to purple for MFM-500(Co). The original phase can be recovered by exposing the dehydrated samples to air (or water vapor), suggesting a reversible change in the coordinated water molecules upon dehydration/rehydration. This is further evidenced by the dehydrated samples remaining intact and stable under a flow of dry O_2. Due to the quality of the data and the complexity of these structures, attempts to determine the crystal structures of the dehydrated phases have thus far been unsuccessful. Samples of desolvated MFM-500(M) (M = Ni, Co) showed very low BET surface areas (<10 m^2/g), as determined from N_2 adsorption isotherms at 77 K.

The proton conductivities of MFM-500(Ni) and MFM-500(Co) were studied by AC impedance spectroscopy. Nyquist

Table 1. Summary of Hydrogen Bond Distances in MFM-500(Co) and MFM-500(Ni)

			MFM-500(Co)				MFM-500(Ni)
D	H	A	*d*(D–H)/Å	*d*(H–A)/Å	*d*(D–A)/Å	D–H–A/°	*d*(D–A)/Å
O1W	H1WA	O34	0.843(10)	2.289(18)	3.013(7)	144(2)	2.972(7)
O1W	H1WA	O34[a]	0.843(10)	2.289(18)	3.013(7)	144(2)	2.972(7)
O2W	H2WA	O33[b]	0.839(10)	2.01(5)	2.726(6)	142(7)	2.716(5)
O33	H33A	O33[d]	0.840(10)	1.62(4)	2.453(7)	170(19)	2.483(7)
O33	H33	O2W[c]	0.838(10)	1.99(8)	2.726(6)	147(13)	2.716(5)

[a] $+x, +y, 1/2 - z$. [b] $1 - y, 1 + x - y, +z$. [c] $+y - x, 1 - x, +z$. [d] $1 - x, 2 - y, 1 - z$.

DOI: 10.1021/jacs.6b02194
J. Am. Chem. Soc. XXXX, XXX, XXX–XXX

plots contain an incomplete semicircle in the high frequency region and a pronounced tail at low frequencies, consistent with blocking of protons at the electrodes (Figure 2). At room

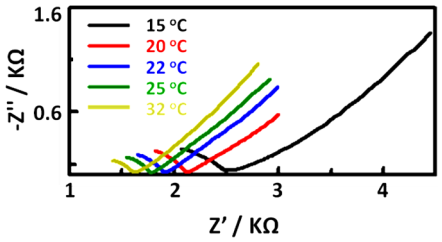

Figure 2. Nyquist plot for MFM-500(Ni) measured at different temperatures and 98% RH.

temperature and 98% RH, the proton conductivities for MFM-500(Ni) and MFM-500(Co) were measured as 4.5×10^{-4} and 4.4×10^{-5} S/cm, respectively. The difference in the conductivities between these isostructural materials probably correlates to the bond strength between coordinated water molecules and the metal cations, as suggested by the TGA plots and solid-state UV/vis absorption spectra (see SI). These values are comparable to those recently reported for MOFs functionalized with phosphonic acid groups under similar conditions. For example, GdHPA-II (HPA = 2-hydroxyphosphonoacetic acid) showed a proton conductivity of 3.2×10^{-4} S/cm at 21 °C and 98% RH, while [Zn-(*m*-H_6L)] [*m*-H_6L = 1,3-bis(aminomethyl)benzene-*N*,*N*′-bis(methylenephosphonic acid)] had a proton conductivity of 1.4×10^{-4} S/cm at 41 °C and 98% RH.[19] More recently, $\{[(Me_2NH_2)_3(SO_4)]_2[Zn_2(ox)_3]\}$ and UiO_{66}-SO_3H showed higher proton conductivities of 4.2×10^{-2} S/cm at 25 °C and 98% RH and 3.4×10^{-3} S/cm at 30 °C and 97% RH, respectively.[20] Impedance data were also measured at 98%, 75%, 45%, and 0% RH at 25 °C for MFM-500(Ni) and MFM-500(Co); both materials showed a steady decrease of conductivity with decreasing %RH (Figures S6 and S7; Table S5). At 0% RH both materials showed no apparent conductivity ($<10^{-9}$ S/cm). This is typically observed for water-mediated proton conductors. It is worth noting that the dehydrated materials show no apparent proton conductivity, and their conductivities (4.5×10^{-4} and 4.4×10^{-5} S/cm for the Ni and Co compounds, respectively) can be recovered by exposing the dehydrated samples to water vapor, consistent with the reversible phase change shown by the *in situ* PXRD data.

The activation energy (E_a) of the proton conduction in MFM-500(Ni) was estimated from the impedance spectra recorded at 98% RH between 15 and 32 °C to be 0.43 eV (Figure S8). Two main mechanisms for proton diffusion are the Vehicle mechanism (typically $E_a > 0.4$ eV) and the Grotthuss mechanism (typically $E_a < 0.4$ eV).[8] For MFM-500(Ni) E_a lies at the boundary of the two mechanisms, indicating that it is likely that proton conduction in MFM-500(Ni) is governed by an intermediate process between the Grotthuss and Vehicle mechanisms. This behavior has been reported in a few cases.[2,21,22] For example, $(NH_4)_2(adp)[Zn_2(ox)_3]\cdot 3H_2O$ (adp = adipic acid; ox^{2-} = oxalate) showed a high proton conductivity of 8×10^{-3} S/cm at 25 °C under 98% RH with $E_a = 0.63$ eV, and the mechanism of proton conduction was assigned as mixed Grotthuss and Vehicle types.[21,22]

We sought to gain further understanding of the mechanism of proton conduction in MFM-500(Ni) using QENS. Data for MFM-500(Ni) were collected between −23 and 150 °C under both anhydrous and 98% RH conditions to study the dynamics of protons through the framework lattice. The elastic incoherent structure factors (EISF) were extracted from the QENS spectra to gain the geometrical information on the molecular motions of active protons in MFM-500(Ni) (see SI). The EISF plots showed clear *Q*-dependence and were carefully fitted with all well-known theoretical models for proton diffusion (i.e., jumping between *n* sites and various free diffusion models as shown in Figure S10). It has been found that the proton diffusion in MFM-500(Ni) is best described by the model of "free diffusion inside a sphere" (eq 1) rather than

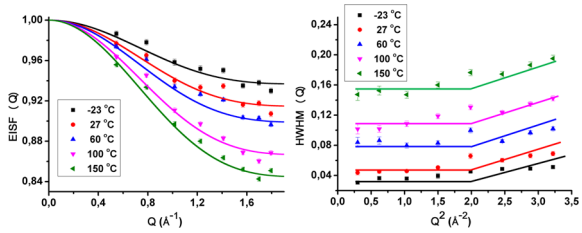

Figure 3. (a) View of the elastic incoherent structure factor (EISF) of MFM-500(Ni). Solid curves represent the simulated EISF based on function (eq 1) for the model of "free diffusion inside a sphere" at different temperatures. (b) Q^2-dependence of the half-width of the half-maximum (HWHM) estimated from the fitting of the data for MFM-500(Ni). Lines are a guide to the eye.

the model of jumping between *n* sites (Figures 3a and S10).[23−25]

$$\mathrm{EISF} = p + (1 - p)[(3j_1(Qr)/(Qr)]^2 \quad (1)$$

where j_1 is the first-order spherical Bessel function, *r* is the radius of the sphere, and *p* and $(1 - p)$ are the immobile and mobile fractions of the protons involved in this process, respectively. The best fitting to EISF plot was observed for $r = 2.25$ Å (Figure S11), entirely consistent with the observed H··· A distances from the single-crystal X-ray structure (taking an O−H bond distance of ∼0.84 Å). The dependency of the spherical free diffusion on the distance *r* is confirmed by the extraction of the half-width of the half-maximum (HWHM, Γ) of the QENS spectra as a function of Q^2 at different temperatures (Figure 3b).[24,26] For $Q^2 > 1.95$ Å^{-2} (corresponding to $r \leq 2.25$ Å), Γ increases with Q^2, indicating free diffusion of protons within a distance of 2.25 Å. For $Q^2 < 1.95$ Å^{-2} (corresponding to $r > 2.25$ Å), Γ does not have any dependency on Q^2, suggesting a confined motion at distances >2.25 Å. This is entirely reasonable because, when the distances are >2.25 Å, the proton conduction needs to be assisted by additional water molecules (or other vehicle molecules), i.e., the origin for the presence of the cooperated Grotthuss and Vehicle mechanisms. QENS data of MFM-500(Ni) recorded under humid conditions confirm that the proton diffusion remains as "free diffusion inside a sphere" with the same diffusion distance $r = 2.25$ Å (Figure S12).

In conclusion, we have combined the single-crystal XRD and QENS spectroscopy to study the molecular mechanism for proton conduction in a new phosphonate-based MOF material. These complementary static and dynamic approaches yield highly consistent results and afford direct visualization of the pathway and mechanisms of proton transfer in the framework

DOI: 10.1021/jacs.6b02194
J. Am. Chem. Soc. XXXX, XXX, XXX−XXX

lattice. For the first time, the model of "free diffusion inside a sphere" has been experimentally confirmed in proton-conducting MOFs. Further efforts to optimize the hydrogen-bonding network in these materials via ligand modification and post-synthetic approaches are currently underway.

■ ASSOCIATED CONTENT

Supporting Information

The Supporting Information is available free of charge on the ACS Publications website at DOI: 10.1021/jacs.6b02194. CCDC-1450010 and CCDC-1450011 contain the supplementary crystallographic data for this paper.

Synthesis procedures, characterization, impedance analysis, and QENS analysis (PDF)
X-ray crystallographic data for MFM-500(Co) (CIF)
X-ray crystallographic data for MFM-500(Ni) (CIF)

■ AUTHOR INFORMATION

Corresponding Authors

*sihai.yang@manchester.ac.uk
*m.schroder@manchester.ac.uk

Notes

The authors declare no competing financial interest.

■ ACKNOWLEDGMENTS

We thank Universities of Manchester and Nottingham and EPSRC for funding. We are especially grateful to STFC and the ISIS Facility for access to Beamline IRIS, and to Diamond Light Source for access to Beamlines I11 and I19. M.S. thanks the ERC for an Advanced Grant.

■ REFERENCES

(1) Yoon, M.; Suh, K.; Natarajan, S.; Kim, K. *Angew. Chem., Int. Ed.* **2013**, *52*, 2688.
(2) Liang, X.; Zhang, F.; Feng, W.; Zou, X.; Zhao, C.; Na, H.; Liu, C.; Sun, F.; Zhu, G. *Chem. Sci.* **2013**, *4*, 983.
(3) (a) Tsai, C. H.; Wang, C. C.; Chang, C. Y.; Lin, C. H.; Yang, Y. W. *Int. J. Hydrogen Energy* **2014**, *39*, 15696. (b) Phang, W. J.; Jo, H.; Lee, W. R.; Song, J. H.; Yoo, K.; Kim, B. S.; Hong, C. S. *Angew. Chem., Int. Ed.* **2015**, *54*, 5142.
(4) (a) Sahoo, S. C.; Kundu, T.; Banerjee, R. *J. Am. Chem. Soc.* **2011**, *133*, 17950. (b) Taylor, J. M.; Mah, R. K.; Moudrakovski, I. L.; Ratcliffe, C. I.; Vaidhyanathan, R.; Shimizu, G. K. H. *J. Am. Chem. Soc.* **2010**, *132*, 14055. (c) Taylor, J. M.; Dawson, K. W.; Shimizu, G. K. H. *J. Am. Chem. Soc.* **2013**, *135*, 1193.
(5) (a) Yang, W.; Lin, X.; Jia, J.; Blake, A. J.; Wilson, C.; Hubberstey, P.; Champness, N. R.; Schröder, M. *Chem. Commun.* **2008**, *3*, 359. (b) Jia, J.; Lin, X.; Wilson, C.; Blake, A. J.; Champness, N. R.; Hubberstey, P.; Walker, G.; Cussen, E. J.; Schröder, M. *Chem. Commun.* **2007**, *3*, 840. (c) Suh, M. P.; Park, H. J.; Prasad, T. K.; Lim, D. *Chem. Rev.* **2012**, *112*, 782. (d) Dailly, A.; Poirier, E. *Energy Environ. Sci.* **2011**, *4*, 3527. (e) Yan, Y.; Lin, X.; Yang, S.; Blake, A. J.; Dailly, A.; Champness, N. R.; Hubberstey, P.; Schröder, M. *Chem. Commun.* **2009**, *9*, 1025. (f) Farha, O. K.; Yazaydın, A. Ö.; Eryazici, I.; Malliakas, C. D.; Hauser, B. G.; Kanatzidis, M. G.; Nguyen, S. T.; Snurr, R. Q.; Hupp, J. T. *Nat. Chem.* **2010**, *2*, 944. (g) Yan, Y.; Telepeni, I.; Yang, S.; Lin, X.; Kockelmann, W.; Dailly, A.; Blake, A. J.; Lewis, W.; Walker, G. S.; Allan, D. R.; Barnett, S. A.; Champness, N. R.; Schröder, M. *J. Am. Chem. Soc.* **2010**, *132*, 4092.
(6) Yang, S.; Sun, J.; Ramirez-Cuesta, A. J.; Callear, S. K.; David, W. I. F.; Anderson, D. P.; Newby, R.; Blake, A. J.; Parker, J. E.; Tang, C. C.; Schröder, M. *Nat. Chem.* **2012**, *4*, 887.
(7) Li, J.; Sculley, J.; Zhou, H. *Chem. Rev.* **2012**, *112*, 869.
(8) Ramaswamy, P.; Wong, N. E.; Shimizu, G. K. H. *Chem. Soc. Rev.* **2014**, *43*, 5913.
(9) Horike, S.; Umeyama, D.; Kitagawa, S. *Acc. Chem. Res.* **2013**, *46*, 2376.
(10) Shigematsu, A.; Yamada, T.; Kitagawa, H. *J. Am. Chem. Soc.* **2011**, *133*, 2034.
(11) Kim, S.; Dawson, K. W.; Gelfand, B. S.; Taylor, J. M.; Shimizu, G. K. H. *J. Am. Chem. Soc.* **2013**, *135*, 963.
(12) Bazaga-Garcia, M.; Colodrero, R. M. P.; Papadaki, M.; Garczarek, P.; Zon, J.; Olivera-Pastor, P.; Losilla, E. R.; Leon-Reina, L.; Aranda, M. A. G.; et al. *J. Am. Chem. Soc.* **2014**, *136*, 5731.
(13) Bureekaew, S.; Horike, S.; Higuchi, M.; Mizuno, M.; Kawamura, T.; Tanaka, D.; Yanai, N.; Kitagawa, S. *Nat. Mater.* **2009**, *8*, 831.
(14) (a) Hurd, J.; Vaidhyanathan, R.; Thangadurai, V.; Ratcliffe, C. I.; Moudrakovski, I. L.; Shimizu, G. K. H. *Nat. Chem.* **2009**, *1*, 705. (b) Umeyama, D.; Horike, S.; Inukai, M.; Kitagawa, S. *J. Am. Chem. Soc.* **2013**, *135*, 11345.
(15) Liu, S.; Yue, Z.; Liu, Y. *Dalton Trans.* **2015**, *44*, 12976.
(16) (a) Begum, S.; Wang, Z.; Donnadio, A.; Costantino, F.; Casciola, M.; Valiullin, R.; Chmelik, C.; Bertmer, M.; Kärger, J.; Haase, J.; Krautscheid, H. *Chem. - Eur. J.* **2014**, *20*, 8862. (b) Miyatsu, S.; Kofu, M.; Nagoe, A.; Yamada, T.; Sadakiyo, M.; Yamada, T.; Kitagawa, H.; Tyagi, M.; García-Sakai, V.; Yamamuro, O. *Phys. Chem. Chem. Phys.* **2014**, *16*, 17295. (c) Horike, S.; Kamitsubo, Y.; Inukai, M.; Fukushima, T.; Umeyama, D.; Itakura, T.; Kitagawa, S. *J. Am. Chem. Soc.* **2013**, *135*, 4612.
(17) (a) Jobic, H.; Ernst, H.; Heink, W.; Kärger, J.; Tuel, A.; Bée, M. *Microporous Mesoporous Mater.* **1998**, *26*, 67. (b) Bedouret, L.; Judeinstein, P.; Ollivier, J.; Combet, J.; Desmedt, A. *J. Phys. Chem. B* **2014**, *118*, 13357. (c) Perrin, J. C.; Lyonnard, S.; Volino, F. *J. Phys. Chem. C* **2007**, *111*, 3393.
(18) Beckmann, J.; Rüttinger, R.; Schwich, T. *Cryst. Growth Des.* **2008**, *8*, 3271.
(19) (a) Colodrero, R. M. P.; Papathanasiou, K. E.; Stavgianoudaki, N.; Olivera-Pastor, P.; Losilla, E. R.; Aranda, M. A. G.; León-Reina, L.; Sanz, J.; Sobrados, I.; Choquesillo-Lazarte, D.; García-Ruiz, J. M.; Atienzar, P.; Rey, F.; Demadis, K. D.; Cabeza, A. *Chem. Mater.* **2012**, *24*, 3780. (b) Colodrero, R. M. P.; Angeli, G. K.; Bazaga-Garcia, M.; Olivera-Pastor, P.; Villemin, D.; Losilla, E. R.; Martos, E. Q.; Hix, G. B.; Aranda, M. A. G.; Demadis, K. D.; Cabeza, A. *Inorg. Chem.* **2013**, *52*, 8770.
(20) (a) Nagarkar, S. S.; Unni, S. M.; Sharma, A.; Kurungot, S.; Ghosh, S. K. *Angew. Chem., Int. Ed.* **2014**, *53*, 2638. (b) Phang, W. P.; Jo, H.; Lee, W. R.; Song, J. H.; Yoo, K.; Kim, B. S.; Hong, C. S. *Angew. Chem., Int. Ed.* **2015**, *54*, 5142.
(21) Sadakiyo, M.; Yamada, T.; Kitagawa, H. *J. Am. Chem. Soc.* **2009**, *131*, 9906.
(22) Sadakiyo, M.; Yamada, T.; Kitagawa, H. *J. Am. Chem. Soc.* **2014**, *136*, 13166.
(23) Russo, D.; Pérez, J.; Zanotti, J.-M.; Desmadril, M.; Durand, D. *Biophys. J.* **2002**, *83*, 2792.
(24) Volino, F.; Dianoux, A. J. *Mol. Phys.* **1980**, *41*, 271.
(25) Bee, M. *Quasielastic Neutron Scattering*; Adam Hilger: Bristol, 1988.
(26) Mukhopadhyay, R.; Mitra, S. *Indian J. Pure Appl. Phys.* **2006**, *44*, 732.

DOI: 10.1021/jacs.6b02194
J. Am. Chem. Soc. XXXX, XXX, XXX−XXX